Insights into the Self-Directed Structuring of Hybrid Organic−Inorganic Silicas through Infrared Studies

Jean-Louis Bantignies,*,† Luc Vellutini,‡ David Maurin,† Patrick Hermet,† Philippe Dieudonné,† Michel Wong Chi Man,*,‡ John R. Bartlett,§ Catherine Bied,‡ Jean-Louis Sauvajol,† and Joël J. E. Moreau‡

Laboratoire des Colloïdes, Verres et Nanomatériaux (UMR CNRS 5587), Université Montpellier II, 34095 Montpellier Cedex 5, France, Laboratoire Hétérochimie Moléculaire et Macromoléculaire (UMR CNRS 5076), Ecole Nationale Supérieure de Chimie de Montpellier, 8 rue de l'école normale, 34296 Montpellier Cedex 5, France, and Australian Nuclear Science and Technology Organisation, Private Mail Bag 1, Menai NSW 2234, Australia

Received: February 15, 2006; In Final Form: June 19, 2006

Fourier transform infrared (FTIR) spectroscopy has been used to probe the organization of the organic fragments in lamellar bridged silsesquioxanes with organic substructures based on alkylene chains of various lengths and urea groups [$O_{1.5}Si(CH_2)_3NHCONH(CH_2)_nNHCONH(CH_2)_3SiO_{1.5}$] ($n$ = 6, 8−12). The structure and intermolecular interactions (hydrophobic and H-bonding) of these well-defined self-structured hybrid silicas are discussed in relation to their powder X-ray diffraction patterns. The degree of structural order is determined by the length and parity of the alkylene spacer. A concomitant enhancement in the degree of condensation of the inorganic component and a decrease in the strength of the hydrophobic interactions between the organic components are demonstrated. The strength and directionality of the H-bonding are directly correlated to the crystalllinity of the organic−inorganic hybrid materials.

1. Introduction

The use of sol−gel processing for synthesizing organobridged trialkoxysilanes[1,2] is an interesting bottom-up approach to new functional hybrid materials with many applications.[3] The recent advances in the structuring of the resulting bridged silsesquioxanes[4−7] represent an important breakthrough in the field of hierarchically organized hybrid materials. We recently reported a new synthetic route to bridged silsesquioxanes with controlled shapes[5] and nanostructures[4] from the acid- or base-catalyzed hydrolysis of a family of silanes based on the structural motif illustrated in Scheme 1. This method mainly relies on the ability of the urea group to self-assemble into well-defined supramolecular architectures through strong hydrogen bonding interactions with adjacent urea moieties.[8] In addition, the organic substructure plays a crucial role in mediating the formation of novel shapes such as helical fibers with chiral morphologies[5a] or plates with flexible or rigid groups.[4] These latter materials were obtained by an acid-catalyzed hydrolysis of the precursors in a large excess of water. In the case of long alkyl chains (n = 10−12) as flexible organic fragments, layered hybrid materials could be obtained.[4a] The interlamellar distance observed was unambiguously related to the size of the organic units. For the precursors with shorter hydrocarbon units (n = 6, 8, 9), the resulting hybrids were less organized and the hydrolysis of the shortest chain length precursor (n = 6) even led to an amorphous solid, as evidenced by their powder X-ray diffraction (PXRD) patterns.

SCHEME 1: Self-Assembled Bridged Silsesquioxanes

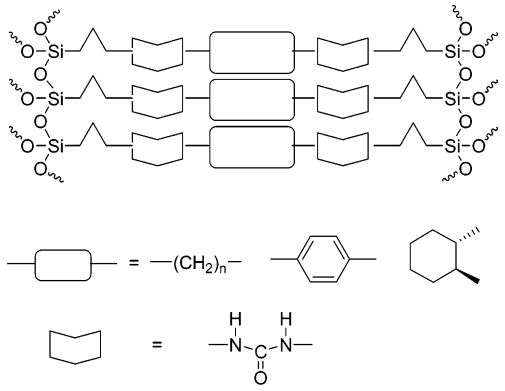

The kinetics of the sol−gel chemistry (hydrolysis−condensation) of the silicon alkoxy groups (which control the formation of the inorganic siloxane network) compete with the noncovalent (thermodynamic) interactions within the self-assembling organic substructure to control the organization and structure of the organic−inorganic hybrids. These latter interactions are predominantly H-bonding between the urea groups and van der Waals (VDW) interactions between the alkyl chains. It therefore appears necessary to understand the fundamental role of the noncovalent interactions in modulating the structure of the materials. Fourier transform infrared (FTIR) spectroscopy is a powerful technique for probing such localized interactions, and the nature of the important H-bonding interactions within the organic fragments can be readily studied by monitoring the amide 1 and amide 2 band positions and the stretching modes of the N−H bonds (νNH).[9,10]

In this paper, we report a study of the influence of noncovalent interactions (particularly H-bonding and VDW interac-

* To whom correspondence should be addressed. E-mail: jean-louis.bantignies@lcvn.univ-Montp2.fr (J.-L.B.); michel.wong-chi-man@enscm.fr (M.W.C.M.). Phone: 33 467 144 639 (J.-L.B.); 33 467 147 219 (M.W.C.M.). Fax: 33 467 144 637 (J.-L.B.); 33 467 144 353 (M.W.C.M.).
† Université Montpellier II.
‡ Ecole Nationale Supérieure de Chimie de Montpellier.
§ Australian Nuclear Science and Technology Organisation.

10.1021/jp060975r CCC: $33.50
Published on Web 07/27/2006

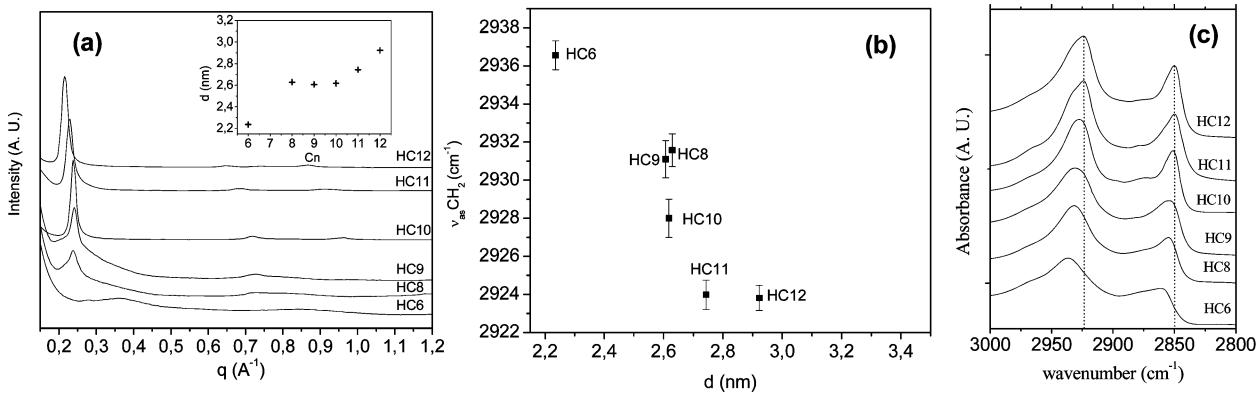

Figure 1. (a) PXRD diagrams of the hybrid materials, $\mathbf{HC}_n$ (n = 6, 8−12). Inset: dependence of the interplane distance, d, as a function of the chain length, C_n. (b) Dependence of $\nu_{as}(CH_2)$ with the interplane distance, d. (c) Infrared spectra of the different hybrid materials in the region of the methylene stretching bands.

tions) in modulating the structure of urea based alkylene bridged silsesquioxanes, using infrared experiments.

2. Experimental Section

2.1. Synthesis of Lamellar Hybrid Silicas. The synthesis of the bis-trialkoxysilylated molecular precursors $(EtO)_3Si-(CH_2)_3NHCONH-(CH_2)_n-NHCONH(CH_2)_3Si(OEt)_3$, $\mathbf{P}_n$ (n = 6, 8−12), and the corresponding hybrids, $\mathbf{HC}n$ (n = 6, 8−12), has already been described.[4c] The hybrids $\mathbf{HC}n$ (n = 8−12) show a long range order, whereas $\mathbf{HC_6}$ is amorphous.

2.2. Synthesis of the Amorphous Hybrid $\mathbf{AC_{10}}$. The molecular precursor with n = 10 ($\mathbf{P_{10}}$) was used to form an amorphous hybrid material, $\mathbf{AC_{10}}$, for comparison with the corresponding lamellar hybrid ($\mathbf{HC_{10}}$). $\mathbf{P_{10}}$, ethanol, distilled water, and NH_4F were introduced into a flask in the following molar ratio: $\mathbf{P_{10}}$, 1; EtOH, 60; H_2O, 6; NH_4F, 0.01. The reaction mixture was left standing under static conditions at room temperature. A gel formed after 2 days, which was then aged for an additional 2 days. It was then ground using a mortar and pestle and washed successively with ethanol and acetone, and the resulting white powder was dried in an oven (110 °C) overnight. FTIR (KBr pellets): 3381 (ν_{NH}), 2932 (ν_{CHas}), 2857 (ν_{CHs}), 1645 (ν_{CO}), 1573 (δ_{NH}), 1132 and 1030 (ν_{SiO}), 923 (ν_{SiOH}). Solid state ^{13}C CP-MAS NMR: δ 159.9, 41.4, 30.0, 18.8, 10.3. Solid state ^{29}Si CP-MAS NMR: δ −65.9 (T^3 units), −59.0 (T^2 units).

2.3. IR Spectroscopy. Mid-infrared transmittance measurements (400−4000 cm^{-1}) were carried out on a Bruker IFS 113V spectrometer equipped with a N_2-cooled mercury cadmium telluride (MCT) detector, a Globar source, and a KBr beam splitter. The spectral resolution was 2 cm^{-1}, and 64 scans were coadded for each spectrum. Since the peaks are wide, the bar of relative error at the maxima of the peak corresponds to the width of the maximum intensity plateau of this peak. Spectra were obtained at sample temperatures of 10−300 K (±1 K) in steps of 30 K using a liquid helium cryostat. KBr pellets were made: a mixture of 1.2 mg of hybrid silica and 300 mg of KBr was stirred and then pressed under 5 tons to form a pellet die.

Room temperature polarized measurements were made using an attenuated total reflection (ATR) accessory with a diamond crystal as the internal reflectance element, which produces an effective angle of incidence of 46°. Single beam spectra were the result of coadding 128 interferograms. The spectral resolution was 1 cm^{-1}. A moderate pressure was applied on the samples, which induced a preferential orientation of the layered hybrid parallel to the ATR prism surface. The spectra were recorded in perpendicular (P) and parallel (L) polarization modes. The L polarization refers to spectra obtained with the electric field vector parallel to the surface of the diamond crystal, whereas the P polarization refers to spectra obtained with the electric field vector at 45° to the surface of the diamond crystal.

The spectra are not smoothed, and no baseline correction is performed. The given frequency corresponds to the middle of the error bar. Given the complex shape of peaks, it was not intended to make fits to draw out a frequency which would have been very model dependent.

3. Results and Discussion

3.1. Conformation of the Alkyl Chain. As shown by powder X-ray diffraction (PXRD), the hybrid materials containing long chains (n > 9) are characterized by a long range order between parallel planes corresponding to a lamellar structure.[4a] The dependence of the interplane distance, d, on the length of the alkyl spacer is presented in Figure 1a, and the X-ray pattern of the amorphous $\mathbf{HC_6}$ compound is given for comparison. The slight variation of d for hybrids $\mathbf{HC}_n$, n < 10 (inset of Figure 1a), suggests that the length of the spacer is not simply correlated to the lamellar distance. Other parameters such as the conformation and the orientation of the alkyl spacer may contribute to the interlamellar distance, and these can be conveniently probed using infrared spectroscopy.[10,11]

3.1.1. Methylene Stretching Bands ($\nu_s(CH_2)$ and $\nu_{as}(CH_2)$). It was reported that the frequency, width, and intensity of the antisymmetric ($\nu_{as}(CH_2)$) and symmetric ($\nu_s(CH_2)$) methylene stretching bands near 2920 and 2850 cm^{-1} are sensitive to the gauche/trans conformer ratio and to the packing density of alkylene chains.[10,12] Previous investigations performed on intercalated clays have revealed that the softening of the $\nu_{as}(CH_2)$ band reflects a highly ordered, all-trans conformation of the alkylene chain. In contrast, a stiffening and broadening of the $\nu_{as}(CH_2)$ band is evidence of the increasing chain disorder. For example, organosilicates containing a C_{12} alkylene chain with liquid crystalline (LC) orientational ordering exhibit a band at 2923 cm^{-1} (Figure 1b). In contrast, this mode shifts to 2936 cm^{-1} in the materials based on a C_6 motif, where the chains are in a liquidlike environment.[10]

The infrared active methylene stretching bands following the chain length of the hybrids are plotted in Figure 1c. These bands are observed around 2850 cm^{-1} ($\nu_s(CH_2)$) and 2925 cm^{-1} ($\nu_{as}(CH_2)$) for $\mathbf{HC_{12}}$ and systematically increase in energy with decreasing C_n length. The relationship between $\nu_{as}(CH_2)$ and the interplane distance, d, is shown in Figure 1b. The positions of $\mathbf{HC_{12}}$ and $\mathbf{HC_{11}}$ are essentially identical, whereas a gradual shift toward higher frequency is observed with decreasing chain

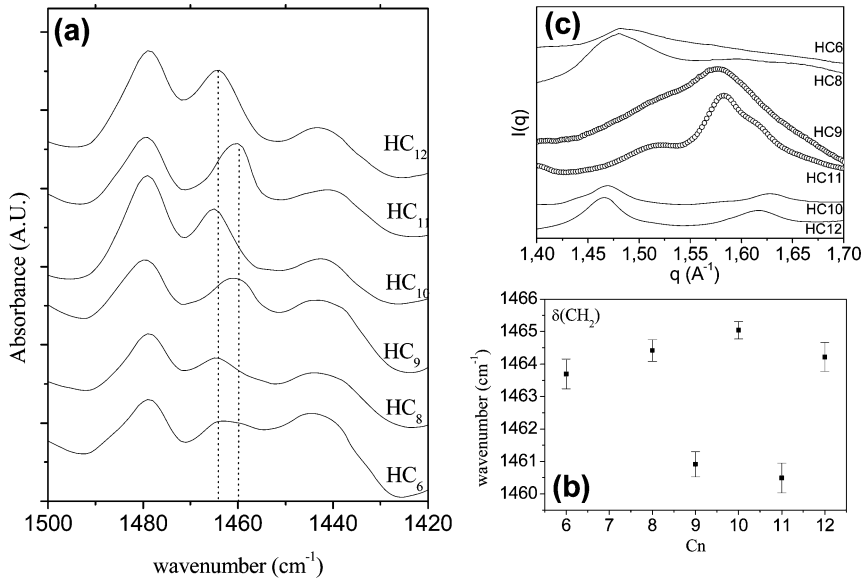

Figure 2. Infrared spectra in the region of the $\delta(CH_2)$ vibrations as a function of the chain length of C_n. (b) Peak frequency dependence of $\delta(CH_2)$ with C_n. (c) PXRD data in the region from 1.4 to 1.7 $Å^{-1}$ as a function of C_n.

length from **HC$_{10}$** to **HC$_6$**. The observed trends in the $\nu_{as}(CH_2)$ frequency suggest that the alkylene chain appears to be in a less ordered state in the hybrids for which $\boldsymbol{n} < 11$ than for **HC$_{11}$** and **HC$_{12}$**. It appears clearly that the $\nu_{as}(CH_2)$ frequency is more sensitive to the structure than to the interlamellar distance.

On the basis of conventional models, which correlate the interlayer structure to the chain length and packing density, a decrease of the interplane distance, *d*, with decreasing C_n length is expected.[10,13] The large variation in the position of $\nu_{as}(CH_2)$ with chain length suggests that the chains display different conformations. The results obtained from the PXRD study of the hybrid materials show that shortening C_n induces a gradual decrease in the long range structural ordering,[4d] leading to loss of the lamellar structure in C_6 due to the less hydrophobic character of the shorter alkylene chain (Figure 1a). In contrast, the longer alkylene spacers exhibit more cohesive VDW interactions between the chains, which lead to an increase in the extent of chain ordering and consequently to a more efficient packing. For shorter chain length, the VDW interactions between the chains decrease, leading to a more disordered configuration. This is mainly due to the tendency of the chains to increase their conformational entropy.

3.1.2. CH_2 Bending Vibration ($\delta(CH_2)$). Additional information about the conformation of the alkyl chain is obtained in the region of the CH_2 bending (scissoring) vibration ($\delta(CH_2)$) located in the 1520−1400 cm^{-1} frequency range. This band is sensitive to interchain interactions and to the chain packing.[10] In general, higher frequencies indicate an "ordering" of the methylene chains in an all-trans crystalline state. Conversely, downshift, broadening, and decreasing intensity of the $\delta(CH_2)$ band indicate a decrease in interchain interactions and a corresponding increase in chain motion which is normally associated with a liquid state.[14] Figure 2a depicts the spectra and the peak frequency of these modes as a function of the length of C_n (Figure 2b). The expected decrease in the intensity of the $\delta(CH_2)$ component (centered around 1464 cm^{-1}) as a function of C_n is clearly displayed. Nevertheless, no significant broadening is observed.

Interestingly, the frequency of the $\delta(CH_2)$ mode also appears to exhibit a dependence on the parity of C_n. In particular, the **HC$_n$** materials with odd-numbered chain lengths (**HC$_{11}$** and **HC$_9$**) exhibit a frequency at around 1460 cm^{-1}. In contrast, the **HC$_n$** with even-numbered chain lengths (**HC$_6$**, **HC$_8$**, **HC$_{10}$**, and **HC$_{12}$**) show a band at around 1464 cm^{-1}. These data correlate with the PXRD data observed in the region from 1.4 to 1.7 $Å^{-1}$ (Figure 2c). This wave vector range is sensitive to the structural order inside the lamellae and to the H-bonding (typical H-bond lengths around 4.5 Å). A diffraction peak in the 1.43−1.47 $Å^{-1}$ range is clearly observed for **HC$_n$** with even-numbered *n*. Such a peak is not found for those materials with odd-numbered $\boldsymbol{n}$ (**HC$_{11}$** and **HC$_9$**), and a peak around 1.58 $Å^{-1}$ is obtained in these latter cases. The IR and X-ray results clearly indicate that the carbon parity affects the order in the final materials.

3.2. Hydrogen Bonding Interactions. The strength of H-bonding interactions in such materials can be probed by IR measurements mainly in two different spectral regions: (a) 3300−3500 cm^{-1} (N−H stretching modes, ν(NH)); (b) 1500−1700 cm^{-1} (amide 1 and amide 2 modes, which arise from ν-(CO) and predominantly in-plane N−H bending (δ(NH)), respectively).

3.2.1. N−H Stretching Modes (ν(NH)). The ν(NH) band envelope consists of contributions arising from both free (non-hydrogen-bonded) and hydrogen-bonded species.[15] To obtain better insight into this behavior, a variable temperature FTIR study was performed on the **HC$_{10}$** hybrid, which we compared with the corresponding amorphous **AC$_{10}$** material prepared in ethanol with a stoichiometric amount of water and NH_4F as catalyst.[1,2]

The temperature effect (10−290 K) on the ν(NH) band is displayed in Figure 3a for the **HC$_{10}$** compound and in Figure 3b for the amorphous **AC$_{10}$** sample. In the **HC$_{10}$** lamellar compound, ν(NH) downshifts from 3345 to 3335 cm^{-1} upon cooling. In contrast, for the amorphous **AC$_{10}$** material, there is no significant temperature dependence of the ν(NH) band. For the whole temperature range investigated, the peak maximum is located at around 3379 cm^{-1} and no significant dependence of the profile and width of the band is observed. On the other hand, the N−H stretching mode involved in weakly hydrogen-bonded or non-hydrogen-bonded groups appears at higher frequencies (around 3445 cm^{-1}) than that in the case of strongly hydrogen-bonded groups.[4a]

We analyze these results as the following: (i) The softening of ν(NH) in **HC$_{10}$** upon cooling is attributed to the strengthening

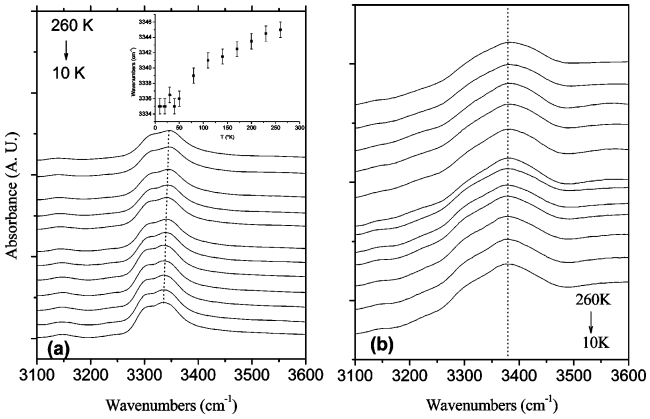

Figure 3. (a) IR spectra of $\mathbf{HC_{10}}$ in the region of the ν(NH) vibrations as a function of temperature between 290 and 10 K. Inset: frequency dependence of ν(NH) with the temperature. (b) IR spectra of $\mathbf{AC_{10}}$ in the region of the ν(NH) vibrations as a function of temperature between 290 and 10 K.

of the hydrogen bonding when the temperature decreases[16] (Figure 3a). (ii) The non-temperature dependence of ν(NH) in $\mathbf{AC_{10}}$ is related to the structural disorder of this material. This implies a spreading of the distribution of the H-bonding strengths and then stronger hydrogen bonds for the lamellar material.

Figure 4a illustrates the change of the room temperature IR spectrum in the region of the ν(NH) stretching band as a function of the chain length. For all $\mathbf{HC}_n$ samples, the spectra display a broad band envelope centered around 3345 cm^{-1}. The position of the band indicates the presence of hydrogen-bonded N−H groups. No significant bands characteristic of free N−H groups centered around 3450 cm^{-1} in solution can be detected.[4a] The shape of the spectrum is complex, and a superposition of ν-(NH) and combination bands (especially ν(CO) + δ(NH) overtones) occurs in this region with possible Fermi resonance between the ν(NH) modes and combination bands.[17] The full width at half-maximum (fwhm) of the ν(NH) band mainly reflects the distribution of the hydrogen bond strength between the urea groups in the material. The dependence of the fwhm of the band on the coherent length extracted from the PXRD interplane feature is shown in Figure 4b. Despite the complex band shape, it is obvious that its width is sensitive to the structural order in the samples. An increase in the length of C_n leads to a corresponding decrease in the fwhm.

The gradual broadening of the ν(NH) bands with decreasing C_n length suggests a spreading of the distribution of the H-bonding strengths as the length of the flexible spacer decreases. This result is in agreement with the structural disorder observed for hybrids with short alkylene spacers.

3.2.2. Amide 1 and Amide 2 Modes. The strength and the directionality of the H-bonding network may be evaluated by comparing the wavenumbers, intensities, and widths of the amide 1, amide 2 (Figure 5a), and N−H bands (Figure 5b) in the ATR spectra of the $\mathbf{HC}_n$ materials obtained in the perpendicular (P) and parallel (L) polarization modes. For $\mathbf{HC}_n$ with $n > 10$, the intensities of the amide 1 band and NH stretching modes are systematically stronger in the L polarization direction than in the corresponding P polarization direction. This suggests that the amide 1 and ν(NH) stretching modes are parallel to the lamellar plane. With decreasing alkyl chain length, this preferential orientation is lost. Thus, the spectral data strongly suggest that both the N−H and C═O groups are preferentially oriented parallel to the lamellar plane for $\mathbf{HC_{10}}$, $\mathbf{HC_{11}}$, and $\mathbf{HC_{12}}$. Additionally, this suggests that the N−H and C═O groups readily form hydrogen bonding networks. In contrast, the hybrids with shorter chain lengths ($\mathbf{HC_9}$, $\mathbf{HC_8}$, and $\mathbf{HC_6}$) exhibit polarization spectra that are almost isotropic.

The frequency difference between the amide 1 and amide 2 bands ($\Delta\nu = (\nu(\mathrm{CO}) - \delta(\mathrm{NH}))$) is commonly used to quantify the average strength of the H-bonding between urea groups,[18] with smaller $\Delta\nu$ values indicating stronger H-bonding. For $\mathbf{HC_{10}}$, $\mathbf{HC_{11}}$, and $\mathbf{HC_{12}}$, the polarization spectra reveal that $\Delta\nu$ is systematically larger in P polarization than in L polarization: from 40 to 35 cm^{-1} (Figure 5c). For $\mathbf{HC_9}$, $\mathbf{HC_8}$, and $\mathbf{HC_6}$, $\Delta\nu$ has no significant trend with the polarization mode. The above results clearly show that the H-bonding interactions are stronger in the direction parallel to the lamellar plane when significant ordering exists in the lamellar hybrids.

From the results discussed above, we suggest a schematic (Figure 6) model illustrating both the directionality of the H-bonding and the effect of alkyl spacer disorder on the structural evolution.

3.3. Sensitivity of the Inorganic Network to the Alkyl Chain Length. Information on the hybrid SiO_2 gel network can be derived from the study of the region containing the Si−O−Si antisymmetric stretching modes (transverse optic (TO) component).[19] The behavior of the infrared absorption spectrum

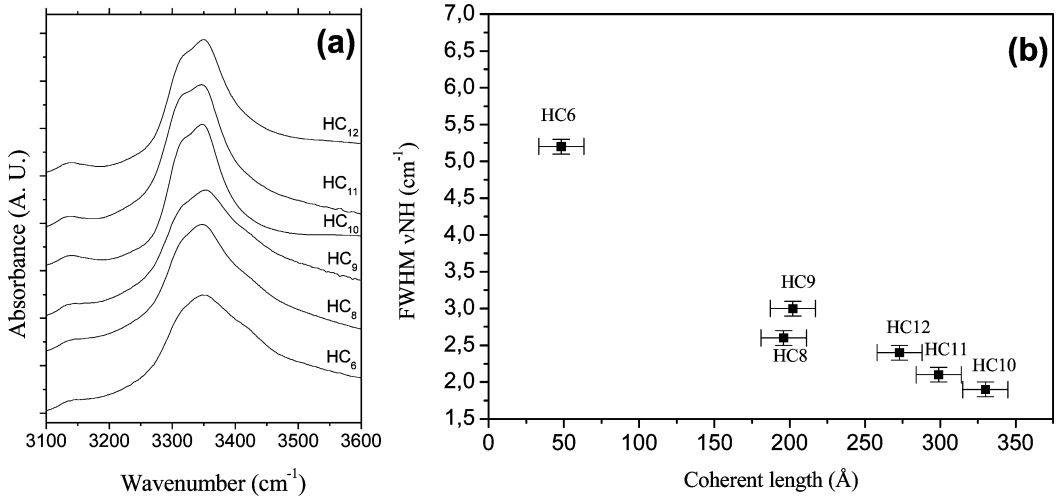

Figure 4. (a) Infrared spectra of the different hybrid materials in the region of the ν(NH) stretching bands. (b) Dependence of the fwhm of the ν(NH) band for the different $\mathbf{HC}_n$ materials on the coherent length extracted from the PXRD interplane feature. Error bar values are calculated from the spatial resolution of the image plate detector (0.002$Å^{-1}$) associated to the pixel size (125 μm).[4d] This corresponds to an error of ±15 Å.

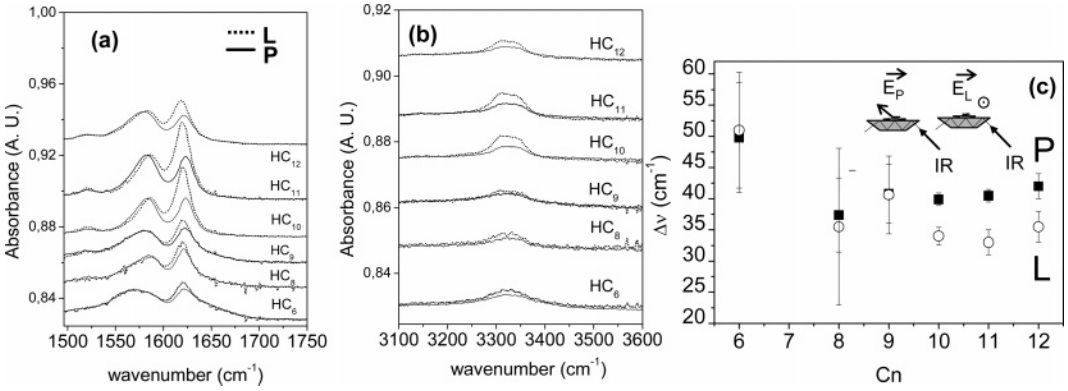

Figure 5. (a) Infrared ATR spectra of the $\mathbf{HC}_n$ materials in the region of the amide 1 and amide 2 bands obtained in the perpendicular (P) and parallel (L) polarization modes. (b) Polarized ATR spectra in the region of the ν(NH) vibrations for the $\mathbf{HC}_n$ materials. (c) Dependence of the frequency difference between the amide 1 and amide 2 bands ($\Delta\nu = (\nu(\mathrm{CO}) - \delta(\mathrm{NH}))$) in P and L polarization with C_n.

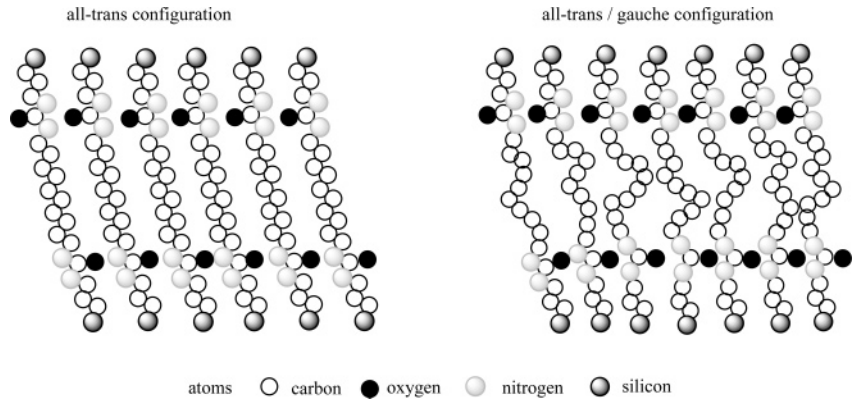

Figure 6. Schematic model for the lamellar hybrid solids showing different conformational states: (left) all-trans conformation; (right) relative amount of gauche conformer.

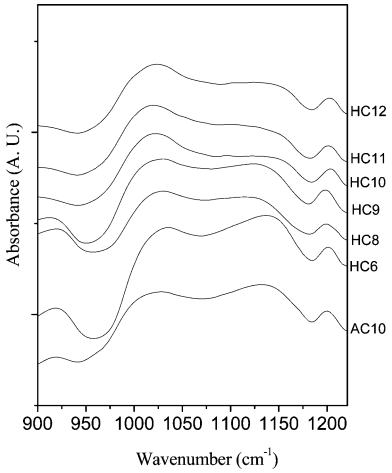

Figure 7. Infrared spectra of the $\mathbf{HC}_n$ materials in the region of the siloxane vibrations.

of $\mathbf{HC}_n$ with the chain length is shown in Figure 7. The absence of the main band of ethanol localized at 880 cm^{-1} suggests that the volatile products of hydrolysis reactions had evaporated as already reported.[20]

The most prominent Si−O−Si asymmetric stretching bands[21] are exhibited at 1025 and 1130 cm^{-1} for all of the $\mathbf{HC}_n$ materials. The intensity ratio of these two bands, $R = I(1130\ cm^{-1})/I(1025\ cm^{-1})$ represents a measure of the state condensation of the gel.[21,22] When the intensity of the 1120−1130 band is higher than that of the 1020−1040 cm^{-1} band (typically $R > 1$), *Tn* cubelike species are favored.[23] In contrast, $R < 1$ values indicate the predominance of open-chain polymeric siloxane (ladderlike oligamers) species. For the amorphous materials $\mathbf{AC_{10}}$ and $\mathbf{HC_6}$, the band located at higher frequencies shows greater intensity than the low frequency counterpart ($R > 1$). This indicates that $\mathbf{AC_{10}}$ and $\mathbf{HC_6}$ materials consist mostly of *Tn* cubelike species. The $\mathbf{HC_8}$ and $\mathbf{HC_9}$ materials, with R close to 1, are mainly dominated by irregular condensation of the cubelike species connected with short ladderlike species.[23] Values of $R < 1$ for $\mathbf{HC_{10}}$, $\mathbf{HC_{11}}$, and $\mathbf{HC_{12}}$ indicate the predominance of open-chain polymeric siloxane species and a much smaller amount of *Tn* cubelike species. A higher degree of condensation is therefore pointed out when C_n decreases. This result is correlated with NMR data showing an increase in the extent of condensation when C_n decreases.[4c] In addition, the position of the lower energy TO peak changes with the C_n length. For $n < 11$, the position of the peak upshifts from 1020 to 1034 cm^{-1} (for $\mathbf{HC_8}$) when the chain length decreases. For the amorphous $\mathbf{HC_6}$ compound, the band is very broad, as expected. This result reflects an increase in the siloxane bond force constant with decreasing n.

4. Conclusions

FTIR analyses have revealed that the long range order in a series of hybrid organic−inorganic silicas, incorporating organic moieties based on urea groups attached to long alkylene chains, is directly related to the structure of the organic fragment. This effect is attributed to the intrinsic self-assembly properties of the organic component, which involve hydrophobic interactions between adjacent alkylene spacers and H-bonding between the urea groups. When the alkylene spacer is sufficiently long, this promotes the formation of a lamellar structure with strong hydrogen bonding interactions and orientational order between the alkylene spacers. This investigation of $\mathbf{HC}_n$ hybrids

demonstrates that the number of methylene groups in the alkylene chain of the alkylene spacer plays a crucial role in the formation of ordered hybrid materials.

Acknowledgment. The CNRS and the Ministère de la recherche de France (ACI Nanosciences-Nanotechnologies) are gratefully acknowledged for funding.

References and Notes

(1) Shea, K. J.; Loy, D. A.; Webster, O. W. *J. Am. Chem. Soc.* **1992**, *114*, 6700−6710.

(2) Corriu, R. J. P.; Moreau, J. J. E.; Thépot, P.; Wong Chi Man, M. *Chem. Mater.* **1992**, *4*, 1217−1224.

(3) (a) Broudic, J.-C.; Conocar, O.; Moreau, J. J. E.; Meyer, D.; Wong Chi Man, M. *J. Mater. Chem.* **1999**, *9*, 2283−2285. (b) Adima, A.; Moreau, J. J. E.; Wong Chi Man, M. *Chirality* **2000**, *12*, 411. (c) Franville, A.-M.; Zambon, D.; Mahiou, R.; Troin, Y. *Chem. Mater.* **2000**, *12*, 428−435. (d) Lebeau, B.; Brasselet, S.; Zyss, J.; Sanchez, C. *Chem. Mater.* **1997**, *9*, 1012−1021.

(4) (a) Moreau, J. J. E.; Vellutini, L.; Wong Chi Man, M.; Bied, C.; Bantignies, J.-L.; Dieudonné, P.; Sauvajol, J.-L. *J. Am. Chem. Soc.* **2001**, *123*, 7957−7958. (b) Moreau, J. J. E.; Pichon, B. P.; Wong Chi Man, M.; Bied, C.; Pritzkow, H.; Bantignies, J.-L.; Dieudonné, P.; Sauvajol, J.-L. *Angew. Chem., Int. Ed.* **2004**, *43*, 203−206. (c) Moreau, J. J. E.; Vellutini, L.; Wong Chi Man, M.; Bied, C.; Bantignies, J.-L.; Dieudonné, P.; Sauvajol, J.-L. *Chem.—Eur. J.* **2005**, *11*, 1527−1537. (d) Moreau, J. J. E.; Vellutini, L.; Dieudonné, P.; Wong Chi Man, M.; Bantignies, J.-L.; Sauvajol, J.-L.; Bied, C. *J. Mater. Chem.* **2005**, *15*, 4943−4948.

(5) (a) Moreau, J. J. E.; Vellutini, L.; Wong Chi Man, M.; Bied, C. *J. Am. Chem. Soc.* **2001**, *123*, 1509−1510. (b) Moreau, J. J. E.; Vellutini, L.; Wong Chi Man, M.; Bied, C. *Chem.—Eur. J.* **2003**, *9*, 1594−1599. (c) Dautel, O.; Lere-Porte, J.-P.; Moreau, J. J. E.; Wong Chi Man, M. *Chem. Commun.* **2003**, 2662−2663.

(6) Boury, B.; Corriu, R. J. P. *Chem. Commun.* **2002**, 795−802.

(7) (a) Inagaki, S.; Guan, S.; Ohsuna, T.; Terasaki, O. *Nature* **2002**, *416*, 304−307. (b) Melde, B. J.; Holland, B. T.; Blanford, C. F.; Stein, A. *Chem. Mater.* **1999**, *11*, 3302−3308. (c) Lu, Y.; Fan, H.; Doke, N.; Loy, D. A.; Assink, R. A.; LaVan, D. A.; Brinker, C. J. *J. Am. Chem. Soc.* **2000**, *122*, 5258−5261.

(8) (a) Simic, V.; Bouteiller, L.; Jalabert, M. *J. Am. Chem. Soc.* **2003**, *125*, 13148−13154. (b) Laan, V. D.; Feringa, B.; Kellogg, R. M.; Esch, V. *Langmuir* **2002**, *18*, 7136−7140.

(9) Jadzyn, J.; Stockhausen, M.; Zywucki, B. *J. Phys. Chem.* **1987**, *91*, 754−757.

(10) Vaia, R. A.; Teukolsky, R. K.; Gianneli, E. P. *Chem. Mater.* **1994**, *6*, 1017−1022.

(11) Singh, S.; Wegmann, J.; Albert, K.; Müller, K. *J. Phys. Chem. B* **2002**, *106*, 878−888.

(12) Snyder, R. G.; Strauss, H. L.; Elliger, C. A. *J. Phys. Chem.* **1982**, *86*, 5145−5150.

(13) Legaly, G. *Solid State Ionics* **1986**, *22*, 43−52.

(14) Weers, J. G.; Scheuing, D. R. In *Fourier Transform Infrared Spectroscopy in Colloid and Interface Science*; Scheuing, D. R., Ed.; ACS Symposium Series 447; American Chemical Society: Washington, DC, 1990; pp 87−122.

(15) Coleman, M. M.; Ho Lee, K.; Skrovanek, D. J.; Painter, P. C. *Macromolecules* **1986**, *19*, 2149−2157.

(16) Mantsch, H. H.; Chapman, D. *Infrared Spectroscopy of Biomolecules*; Wiley & Sons: New York, 1995.

(17) Careri, G.; Buontempo, U.; Galluzzi, F.; Scott, A. C.; Gratton, E.; Shyamsunder, E. *Phys. Rev. B* **1984**, *30* (8), 4689−4702.

(18) Terech, P.; Weiss, R. G. *Chem. Rev.* **1997**, *97*, 3133−3159.

(19) Brinker, C. J.; Scherer, G. W. *Sol−Gel Science*; Academic Press Inc.: Boston, MA, 1990.

(20) Innocenzi P. *J. Non-Cryst. Solids* **2003**, *316*, 310−319.

(21) Zhang, Z.; Wakabayashi, H. *J. Sol−Gel Sci. Technol.* **1998**, *12*, 153−158.

(22) Zhang, Z.; Tanigami, Y.; Terai, R.; Wakabayashi, H. *J. Non-Cryst. Solids* **1995**, *189*, 212−217.

(23) Orel, B.; Jese, R.; Vilcnik, A.; Stangar U. L. *J. Sol−Gel Sci. Technol.* **2005**, *34*, 251−265.